

lobule. Importantly, we combined support vector machine and multiple kernel learning frameworks to fuse multiple levels of network topological features for classification of individuals, achieving high accuracy of 86.47%. Together, our study revealed the disrupted topological organization of structural networks related to pathophysiology of TS, and the discriminative topological features for classification are potential quantitative neuroimaging biomarkers for clinical TS diagnosis. *Hum Brain Mapp* 00:000–000, 2017. © 2017 Wiley Periodicals, Inc.

Key words: Tourette syndrome; diffusion MRI; probabilistic tractography; structural network; graph theory; topological organization; multiple kernel learning

INTRODUCTION

Tourette syndrome (TS) is a childhood-onset neurobehavioral disorder characterized by the presence of multiple motor and vocal tics. The typical age of onset ranges from 5 to 7 years old and the worst tic severity for most patients falls between 7 and 15 years old [Liu et al., 2013b]. Affected individuals typically have repetitive, stereotyped movements or vocalizations, such as blinking, sniffing, facial movements, or tensing of the abdominal musculature [Robertson and Kao, 2011]. TS is frequently accompanied by comorbidities such as obsessive-compulsive disorder (OCD), attention-deficit hyperactivity disorder (ADHD), and other social and behavioral disturbances [Stokes et al., 1991].

The pathophysiological mechanism that produces tics remains elusive. However, previous neuropathological and neuroimaging studies have reported dysfunction of distinct corticobasal ganglia circuits in relation to tic generation [Mink, 2003; Worbe et al., 2012]. Indeed, the dysfunction of corticobasal ganglia circuits at different levels in TS patient were revealed by previous studies. Briefly, cortical structural changes were found in prefrontal, sensorimotor, anterior cingulate, parietal, and temporal regions [Cherine et al., 2010; Muller-Vahl et al., 2009; Peterson et al., 2001; Sowell et al., 2008], with altered volumes of the corpus callosum [Plessen et al., 2004], basal ganglia [Peterson et al., 2003], and thalamus [Miller et al., 2010]. Apart from the macroscopic volumetric changes, several studies pointed to microstructural abnormalities in white matter (WM), which extend beyond motor pathways in TS patients [Neuner et al., 2010, 2011]. Nevertheless, these studies

only revealed TS-related structural alterations in some individual brain regions or circuits, including importantly, a series of parallel cortico-striato-thalamo-cortical (CSTC) circuits that link specific regions of the frontal cortex to subcortical structures and provide a framework for understanding the interconnected neurobiological roots of TS [Felling and Singer, 2011]. In particular, looking at the brain as a complex network comprising highly interconnected brain regions motivates us to study TS-related neurological disorders from a network perspective. The brain structural networks [Sporns et al., 2005] could provide us with an anatomical and physiological substrate of brain functions and help us understand how the brain structures shape functional interactions [Qi et al., 2016]. Therefore, studying WM structural networks has gained a lot of popularity recently, while highlighting the urgent need to quantify WM structural networks *in vivo*, noninvasively, on a global scale, to depict the topological organization of brain structures [Parker et al., 2014]. Subsequently, this may help pin down any neurological disease-related alteration in WM structural networks.

One of the most popular noninvasive imaging techniques is diffusion MRI. This modality reveals the microstructural characteristics of white matter (WM) tracts in the brain. Specifically, diffusion tensor imaging (DTI) and diffusion MRI tractography can reliably reconstruct the major WM tracts, thereby mapping the WM integrity and structural connectivity of the human brain *in vivo* [Basser et al., 1994a, 1994b, 2000]. Many previous studies have utilized the DTI technique and diffusion measures to investigate microstructural changes in TS children [Liu et al., 2013b; Wen et al., 2016a]. These studies have shown that structural connectivity gets disrupted in TS patients in specific WM tracts, involving the prefrontal, parietal, occipital, and subcortical WM. These findings propel the hypothesis that structural connectivity is disrupted in TS.

Although these previous studies have markedly advanced our understanding of WM alterations in TS, it remains unclear as to whether the topological organization (e.g., network global/local efficiency, small-worldness property, and nodal efficiency) of WM structural networks is abnormal in TS children. With the increasing studies reconstructing human whole-brain WM networks using diffusion MRI deterministic or probabilistic tractography

Abbreviations

TS	Tourette syndrome
MRI	magnetic resonance imaging
DTI	diffusion tensor imaging
WM	white matter
SWM	superficial white matter
NBS	network-based statistical
YGTSS	Yale Global Tic Severity Scale
SVM	support vector machine
MKL	multiple kernel learning
MK-SVM	multiple kernel support vector machine

methods [Gong et al., 2009a,b; Iturria-Medina et al., 2008], more interest has been shown for depicting the network-based measurements derived from brain network data. Graph theoretical analysis can provide a unique framework for the measurement of brain networks, so it has gained more popularity in the neuroimaging and brain network research fields. In particular, graph theory analysis revealed that the WM networks exhibit many crucial topological properties, such as highly connected hubs and small worldness [Watts and Strogatz, 1998]. Generally, a small-world network is defined as a network which has high clustering coefficients and short average path lengths [Telesford et al., 2011]. Small worldness is a global network measure that quantifies the balance between integration and segregation among all the nodes in the network [Humphries and Prescott, 2006]. Furthermore, the topological organization of WM networks is disrupted under pathological conditions, for example, Alzheimer’s disease [Lo et al., 2010], schizophrenia [van den Heuvel et al., 2010; Zalesky et al., 2010], attention-deficit hyperactivity disorder (ADHD) [Cao et al., 2013], neuromyelitis optica [Liu et al., 2013a], and multiple sclerosis [Shu et al., 2011]. As for TS, altered activation and functional connectivity in cortico-basal ganglia networks was found using resting-state fMRI data [Werner et al., 2011; Worbe et al., 2012]. In addition, control networks in pediatric TS show immature and anomalous patterns of functional connectivity, primarily found in the frontoparietal network, thought to be important for online adaptive control [Church et al., 2009]. Other studies using diffusion MRI and tractography methods showed altered structural connectivity of corticobasal ganglia networks [Cheng et al., 2014; Worbe et al., 2015] in adult TS patients. However, those studies only revealed functional or structural abnormalities in distinct cortico-basal ganglia circuits, and no study has previously integrated the diffusion MRI tractography method and graph theoretical analysis to examine abnormal topological organization of whole-brain structural networks in TS patients, especially in TS children.

In addition, to date, the studies on TS were mainly limited to using traditional univariate analyses (e.g., *t* tests) to test for group differences. The significant findings (structural or functional alterations) are only at group level which limited clinical application. Therefore, recent attention has turned toward integrating machine learning and neuroimaging techniques to assist clinical diagnosis. Unlike group-based comparison approaches, machine-learning techniques are able to detect the fine-grained spatial discriminative patterns, which are critical for individual-based disease diagnosis [Liu et al., 2014]. Especially, many studies have applied machine learning methods to investigate brain functional or structural networks for assisting clinical disease diagnosis [Dai et al., 2012, 2013; Jie et al., 2014; Jin et al., 2015; Sacchet et al., 2015], however, only a few of them [Greene et al., 2016] are related to TS. To date, there are no reliable neuromarkers for clinical TS diagnosis, and

TS is still misdiagnosed due to its complicated clinical presentation [Cavanna and Seri, 2013]. Therefore, applying machine-learning algorithms to network-based features for diagnostic classification/prediction of individuals will be helpful in assisting eventual clinical diagnosis. Furthermore, the important features used to classify individuals by diagnosis also hold promise for further refinement of the classification methods to ultimately predict prognosis and treatment responses [Greene et al., 2016].

In this study, we used diffusion MRI probabilistic tractography and graph theory to investigate the topological organization of whole-brain structural networks in drug-naive TS and healthy children, and their relation to clinical features. In our study, we used drug-naive subjects to exclude the effects of stimulants, as previous studies have suggested that stimulants can significantly influence the structure and function of central nervous system in TS [Golden, 1977]. In this article, we aimed to investigate whether TS children would show abnormal global and regional topological properties, disrupted nodal efficiency, altered structural connectivity between nodal regions in the whole-brain WM networks and whether these topological changes would significantly correlate with the clinical characteristics of TS children. We assumed that the brain structural network in both TS and healthy children could follow a small-world organization, which was investigated using graph theoretical analysis to identify the differences in global and regional topological properties of brain structural networks between TS and healthy children. We hypothesized that TS children may have a disrupted topological organization of WM structural networks, involving importantly, the basal ganglia and cortical frontal areas, as previous studies revealed that microstructural dysfunction measured by DTI in component regions of the fronto-striato-thalamic (FST) circuit contributes to the pathophysiology in TS [Müller-Vahl et al., 2014; Makki et al., 2008]. Moreover, to enhance our contributions to assisting the clinical TS diagnosis, we investigated using the complementary topological properties (global, nodal, edge) of WM structural networks as features to accurately discriminate TS children from controls. We employed the multiple kernel learning (MKL) frameworks in our previous study [Wen et al., 2017a] to fuse these complementary network-based features, and the most discriminative features for classification, which are highly related to pathophysiology of TS, will be potential important neuroimaging biomarkers for assisting the clinical TS diagnosis.

MATERIALS AND METHODS

Subjects

Forty-four TS patients were recruited from outpatient clinics in Beijing Children’s Hospital from July 2012 to May 2015 (age: 8.98 ± 3.114 years, range: 3–16 years; 11 female). All the patients met DSM-IV-TR (Diagnostic and

TABLE I. Demographic variables and clinical characteristics of TS patients and normal controls

Characteristics		TS (<i>n</i> = 44)	HC (<i>n</i> = 41)	<i>P</i> value	
Sex		33M/11F	26M/15F	0.247 [†]	
Age (range)		8.98 ± 3.11 (3–16 years)	10.27 ± 3.18 (3–15 years)	0.062 [†]	
Concurrent ADHD		7	No	-	
Concurrent OCD		No	No	-	
YGTSS	Motor tics	17.55 ± 3.56	-	-	
	Vocal tics	8.77 ± 7.60	-	-	
	Impairment rating	25.68 ± 12.13	-	-	
Duration (years)		1.73 ± 1.44	-	-	
Head Motion	Translation (mm)	<i>x</i>	0.049 ± 0.045	0.051 ± 0.039	0.804 [†]
		<i>y</i>	0.154 ± 0.058	0.163 ± 0.032	0.393 [†]
<i>z</i>		0.397 ± 0.161	0.362 ± 0.122	0.263 [†]	
	Euclidian distance (mm)	0.406 ± 0.111	0.423 ± 0.133	0.546 [†]	
	Rotation (10 ⁻¹ ×radians)	<i>X</i>	0.023 ± 0.023	0.029 ± 0.025	0.196 [†]
		<i>Y</i>	0.010 ± 0.009	0.013 ± 0.009	0.068 [†]
		<i>Z</i>	0.010 ± 0.007	0.010 ± 0.006	0.558 [†]
	Mean displacement (mm)	abs	0.810 ± 0.199	0.820 ± 0.133	0.768 [†]
		rel	0.299 ± 0.054	0.300 ± 0.056	0.974 [†]

P > 0.05 indicates that age, gender, and all head-motion parameters have no significant between-group differences and are well matched.

abs, absolute; rel, relative. YGTSS, Yale Global Tic Severity Scale; ADHD, attention-deficit hyperactivity disorder; OCD, obsessive-compulsive disorder; M, male; F, female. [†] = χ^2 (chi-square) test.

Statistical Manual of Mental Disorders, 4th Edition, text revision) criteria for TS. We also included 41 age- and gender-matched health controls in our study (age: 10.27 ± 3.18 years; range: 3–15 years; 15 female). The child psychiatrist (chief physician) in our hospital did outpatient interview to make differential diagnosis of psychiatric comorbidities for child subjects, based on the exclusion criteria of psychiatric disorders. The exclusion criteria of psychiatric disorders were established according to the Chinese Classification of Mental Disorders (currently on a third version, the CCMD-3), published by the Chinese Society of Psychiatry (CSP), and used as a clinical guide in China for the diagnosis of mental disorders. The diagnostic criteria of CCMD-3 also refer to the research criteria of DSM-IV [Chen, 2002]. Then the professional neurologists made differential diagnosis of OCD and ADHD using scales. Briefly, we used a clinical interview and the Children’s Yale-Brown Obsessive Compulsive Scale (CY-BOCS) [Scahill et al., 1997] to diagnose OCD and used the German short version of Wender Utah rating scale (WURS-k, translated to Chinese) [Retz-Junginger et al., 2003] to diagnose ADHD. Patients fulfilling OCD criteria or other co-morbidities were excluded from the study. Tic severity for all patients was rated using the Yale Global Tic Severity Scale (YGTSS) [Leckman et al., 1989] and ranged from 10 to 79 ([mean ± SD]: 51.20 ± 19.38). The duration of TS ranged from 3 months to 5 years ([mean ± SD]: 1.73 ± 1.44 years). For subjects who had course <1 year, their diagnosis was made by follow-up call and they were all finally diagnosed exactly as TS by our professional neurologists and psychiatrists. Following the study

approval by Beijing Children’s Hospital review board, written informed consent was obtained from all the parents/guardians according to the Declaration of Helsinki. Details of the patients are shown in Table I.

Data Acquisition

Magnetic resonance imaging was acquired using a 3 T MR scanner (Gyrosan Interna Nova, Philips, Netherland). Head positioning was standardized using canthomeatal landmarks. The head was stabilized with foam pads to minimize head movements. Patients were instructed to suppress tics and minimize head movements during scanning as much as possible. All children under 7 years old were kept asleep during the MR scan. Axial three-dimensional diffusion tensor imaging (DTI) was acquired from all the subjects. DTI was performed using the following protocol: spin-echo diffusion-weighted echo-planar imaging sequence, 2 mm slice thickness, no interslice gap, repetition time = 4300 ms, echo time = 95 ms, field of view (FOV) = 255 × 255 mm, reconstructed image matrix = 336 × 336. Diffusion MRI images were obtained from 30 non-collinear directions with a *b* value of 1000 s/mm². Three-dimensional T1-weighted imaging was performed with axial three-dimensional-Fast Field Echo (3D FFE) sequence with the following parameters: repetition time (TR) = 25 ms, echo time (TE) = 4.6 ms, flip angle = 30°, reconstructed image matrix = 256 × 256, field of view (FOV) = 200 × 200 mm, slice thickness = 1 mm.

TABLE II. Cortical and subcortical regions of interest defined in our study

Regions	Abbr.	Regions	Abbr.
Precentral gyrus	PreCG	Lingual gyrus	LING
Superior frontal gyrus, dorsolateral	SFGdor	Superior occipital gyrus	SOG
Superior frontal gyrus, orbital part	ORBsup	Middle occipital gyrus	MOG
Middle frontal gyrus	MFG	Inferior occipital gyrus	IOG
Middle frontal gyrus orbital part	ORBmid	Fusiform gyrus	FFG
Inferior frontal gyrus, opercular part	IFGoperc	Postcentral gyrus	PoCG
Inferior frontal gyrus, triangular part	IFGtriang	Superior parietal gyrus	SPG
Inferior frontal gyrus, orbital part	ORBinf	Inferior parietal, but supramarginal and angular gyri	IPL
Rolandic operculum	ROL	Supramarginal gyrus	SMG
Supplementary motor area	SMA	Angular gyrus	ANG
Olfactory cortex	OLF	Precuneus	PCUN
Superior frontal gyrus, medial	SFGmed	Paracentral lobule	PCL
Superior frontal gyrus, medial orbital	ORBsupmed	Caudate nucleus	CAU
Gyrus rectus	REC	Lenticular nucleus, putamen	PUT
Insula	INS	Lenticular nucleus, pallidum	PAL
Anterior cingulate and paracingulate gyri	ACG	Thalamus	THA
Median cingulate and paracingulate gyri	DCG	Heschl gyrus	HES
Posterior cingulate gyrus	PCG	Superior temporal gyrus	STG
Hippocampus	HIP	Temporal pole: superior temporal gyrus	TPOsup
Parahippocampal gyrus	PHG	Middle temporal gyrus	MTG
Amygdala	AMY	Temporal pole: middle temporal gyrus	TPOmid
Calcarine fissure and surrounding cortex	CAL	Inferior temporal gyrus	ITG
Cuneus	CUN		

Preprocessing

Following DTI acquisition, we used the FMRIB’s Diffusion Toolbox (FDT2.0) within FSL v4.1 (<http://www.fmrib.ox.ac.uk/fsl>) for DTI processing. As differences in head motion between groups can induce spurious group differences [Yendiki et al., 2014], prior to the estimation of diffusion, we used the same preprocessing pipeline as in the previous TS study [Wen et al., 2016a] to perform corrections for distortions due to eddy currents and head motion. In detail, we used the *eddy* tool in FDT, which is a tool to correct for eddy current-induced distortions and subject movements in diffusion data. It simultaneously models the effects of diffusion eddy currents and movements on the image. It also performs outlier detection to identify slices where signal has been lost as a consequence of subject movement during the diffusion encoding, and permits replacement of the outliers with distortion-free data. For each participant, 30 DTI volumes with 1000 s/mm² *b* value were first affinely registered to the *b*₀ volume. After running motion and eddy correction, we extracted the head motion parameters with the displacement, rotation, and translation information for each subject. We found no significant between-group differences for any head motion parameter using the two-sample *t* test (Table I). Nonbrain voxels were removed using Brain Extraction Tool (BET) of FSL; a fractional intensity threshold of 0.25 was selected, resulting in a brain-extracted 4D image and a binary brain mask for each subject. We then used the eddy-corrected 4D data and corresponding brain mask to fit the diffusion tensor model at each voxel using the FDT.

Eigenvalues of diffusion tensor matrix ($\lambda_1, \lambda_2, \lambda_3$) were obtained and maps of fractional anisotropy (FA) were generated.

Network Construction

Nodes and edges constitute the two basic elements of a network. In this study, we defined all the network nodes and edges using the following steps.

Network node definition

We defined the network nodes strictly in accordance with the procedure described previously [Gong et al., 2009a,b] and was performed here using SPM8 (<http://www.fil.ion.ucl.ac.uk/spm>). Briefly, individual T1-weighted images were co-registered to the *b*₀ images in the DTI space. Then, the transformed T1 images were then nonlinearly transformed to the ICBM152 T1 template in the MNI space. The inverse transformations were used to warp the automated anatomical labeling (AAL) atlas [Tzourio-Mazoyer et al., 2002] from the MNI space to the DTI native space. Of note, the nearest-neighbor interpolation method was used to preserve discrete labeling values. Using this procedure, we obtained 90 cortical and subcortical regions (45 for each hemisphere; Table II), each representing a node in the network (Fig. 1).

Network edge definition

To define the connections (edges) between brain regions, we performed probabilistic tractography using the FMRIB

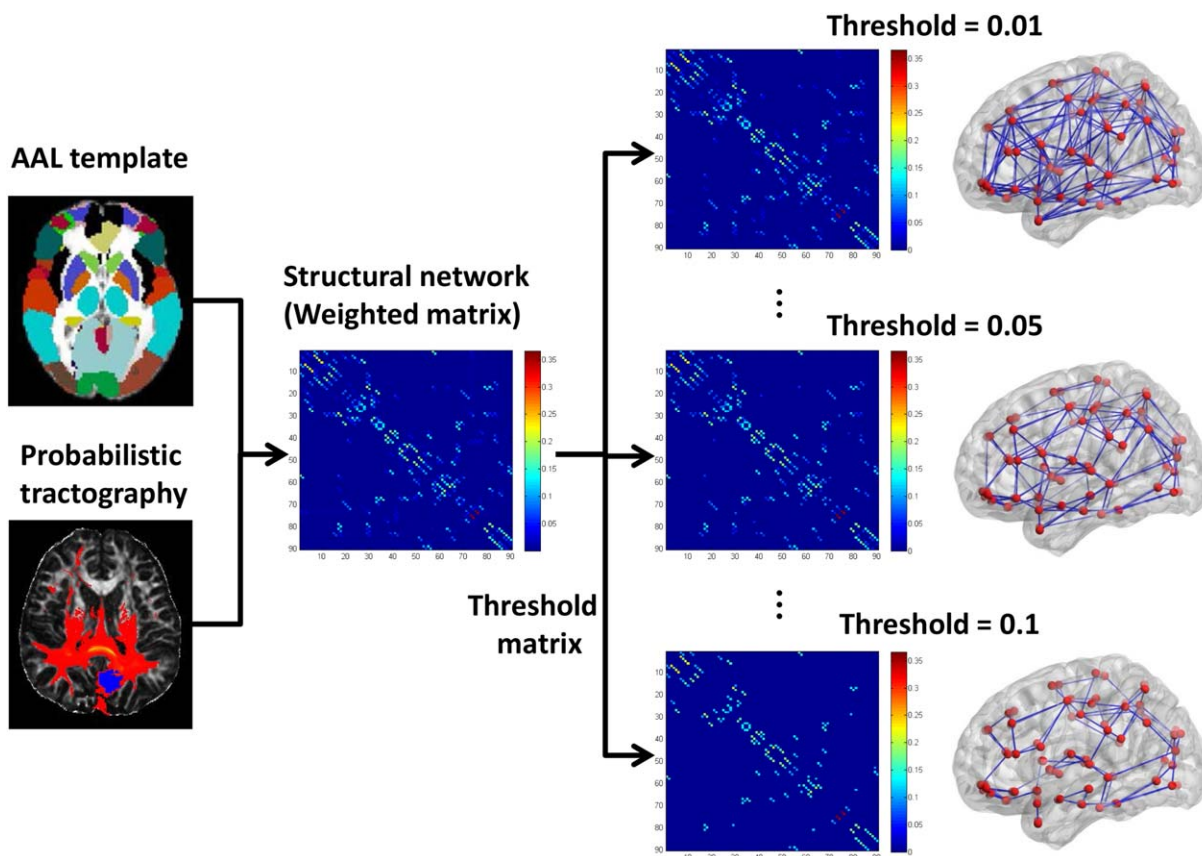


Figure 1.

The flowchart for constructing the WM structural network using diffusion MRI data. [Color figure can be viewed at wileyonlinelibrary.com]

Diffusion Toolbox (FSL, version 4.1; <http://www.fmrib.ox.ac.uk/fsl>). First, we used the `bedpostx` tool in FSL to run Markov Chain Monte Carlo sampling, to estimate distributions on diffusion parameters at each voxel, which allows to model crossing fibers within each voxel of the brain. Second, we used the `probtrackx` tool in FSL to perform probabilistic tracking. Briefly, we repetitively performed 5000 sampling from the distributions of voxel-wise principal diffusion directions, each time computing a streamline through these local samples to generate a probabilistic streamline fiber. For a seed region, $5000 \times n$ streamline fibers were sampled; n is the number of voxels in the seed region. The number of streamline fibers passing through a given region divided by $5000 \times n$ is calculated as the connectivity probability from the seed region to the given region. In our study, each brain region in AAL template was selected as the seed region, and its connectivity probability to each of the other 89 regions was calculated. Notably, the probability from i to j is not necessarily equivalent to the probability from j to i because the tractography is dependent on the seeding location. However, these two probabilities are highly correlated across the brain regions

for all subjects in our study (all Pearson $r > 0.76$, $P < 0.05$). Thus, we defined the unidirectional connectivity P_{ij} between region i and region j by averaging these two probabilities as in Cao et al. [2013].

Finally, to define the network edges, we computed $w_{ij} = P_{ij}$ as the weight between brain regions i and j . For each subject, a 90×90 symmetric-weighted network was constructed. To remove spurious connections, we applied a set of thresholds ranging between 0.01 and 0.1 at equal intervals of 0.0025 empirically based on a previous structural network study [Cao et al., 2013]. Specifically, two brain regions were considered disconnected if the connection weight w_{ij} was below a given threshold. The flowchart for structural network construction was shown in Figure 1.

Network Topological Attributes Analysis

For the weighted WM networks (G) at each threshold, we calculate two sets of network topological attributes, including both global and local network properties. The general descriptions of these network properties are given below.

Global network properties

S_p : *network strength (mean degree)*. S_p is the strength of the network, which is defined as the mean degree of all the regions in the brain network.

E_{glob} : *network global efficiency*. E_{glob} is defined as the inverse of average shortest path length. It reflects the network efficiency in transferring information, which can be computed as follows:

$$E_{glob}(G) = \frac{1}{N(N-1)} \sum_{i \neq j \in G} \frac{1}{L_{ij}} \quad (1)$$

E_{loc} : *network local efficiency*. E_{loc} is defined as the average value of all regions' local efficiency. It reflects system redundancy and tolerance to attack, which can be computed as follows:

$$E_{loc}(G) = \frac{1}{N} \sum_{i \in G} E_{glob}(G_i) \quad (2)$$

L_p : *the shortest path length*. L_{ij} is defined as the length of the path for node i and node j with the shortest length. L_p is the shortest path length of network G , which can be computed as follows:

$$L_p(G) = \frac{1}{N(N-1)} \sum_{i \neq j \in G} L_{ij} \quad (3)$$

C_p : *the clustering coefficient*. $C(i)$ is defined as the clustering coefficient of a node i , equal to the ratio between the existing number of edges among the neighbors of the node i and the maximum possible number of connections among these neighbors, which can be computed as follows:

$$C(i) = \frac{2}{k_i(k_i-1)} \sum_{j,k} (\bar{w}_{ij}\bar{w}_{jk}\bar{w}_{ki})^{\frac{1}{3}} \quad (4)$$

where k_i is the degree of node i and \bar{w}_{ij} is the edge weight, which is scaled by the mean of all edge weights to control each participant's cost at the same level. C_p is defined as the average clustering coefficient over all nodes. It quantifies the cliquishness and reflects the extent of local interconnectivity.

To examine the small-world properties, the C_p and L_p of the brain networks were compared with those of random networks. In this study, we generated 100 matched random networks, which had the same number of nodes, edges, and degree distribution as the real networks [Maslov and Sneppen, 2002]. To preserve the weight distribution of the network, we retained the weight of each edge during the randomization procedure.

λ : *the normalized shortest path length*. $\lambda = L_p^{real}/L_p^{rand}$, L_p^{rand} is the mean shortest path length of 100 matched random networks.

γ : *the normalized clustering coefficient*. $\gamma = C_p^{real}/C_p^{rand}$, C_p^{rand} is the mean clustering coefficient of 100 matched random networks.

σ : *the small worldness*. $\sigma = \gamma/\lambda$, which reflects the balance between integration and segregation among all the nodes in the network. The network with small worldness is a

kind of network with both high clustering coefficient and low shortest path length.

Regional nodal characteristics

$E_{nodal}(i)$: *nodal efficiency*. $E_{nodal}(i)$ is the regional efficiency of node i and indicates the nodal (regional) characteristics of the WM networks, which can be computed as follows:

$$E_{nodal}(i) = \frac{1}{N-1} \sum_{i \neq j \in G} \frac{1}{L_{ij}} \quad (5)$$

where L_{ij} is the shortest path length between node i and node j in the network G , and $E_{nodal}(i)$ measures the average shortest path length between a given node i and all the other nodes in the network.

Similar to previous studies [Zhang et al., 2011, 2015], we also calculated the area under the curve (AUC) for each network metric (global and local topological properties) to provide a summarized scalar independent of single threshold selection. Of note, we used the AUC value of the nodal efficiency across thresholds for the analysis of regional properties, defining brain hubs, and significant altered nodes.

Network-Based Statistical Analysis

To localize specific pairs of brain regions in which structural connectivity was altered in TS children, we used a method called network-based statistical (NBS) analysis [Zalesky et al., 2010] (<http://www.nitrc.org/projects/nbs/>), which identifies the between-group differences in pairwise edge (or connection) weight under a series of probability thresholds (0.01–0.1, interval = 0.0025). The basic idea of the network-based statistics is to correct for multiple comparisons by testing for evidence against the null distribution at the level of graph components, rather than at the level of individual connections [Hong et al., 2014]. Briefly, the two-sample t tests were first performed to test for between-group differences in the connections of the $90 \times (90 - 1)/2 = 4005$ unique regional pairings. Then, a most liberal primary threshold ($P = 0.01$) [Marques et al., 2015; Zhu et al., 2016] in NBS analysis was applied to the t statistic computed for each link to define a set of suprathreshold links, among which any connected components and their size (number of links) were then determined. The t value was uniquely determined, when the degrees of freedom ($N1 - 1 + N2 - 1$ for independent samples, in our study, $41 - 1 + 44 - 1 = 83$), and significance level (P value = 0.01 in our study) were determined. The $t = 2.372$ in our study can be calculated based on the table for T distributions which is provided in Supporting Information. Second, the null distribution of connected component size was derived using a nonparametric permutation approach (10,000 permutations) to estimate the significance for each component, then the threshold ($P = 0.05$) was used to generate suprathreshold links [Cao et al., 2013]. Finally, the corrected P value was

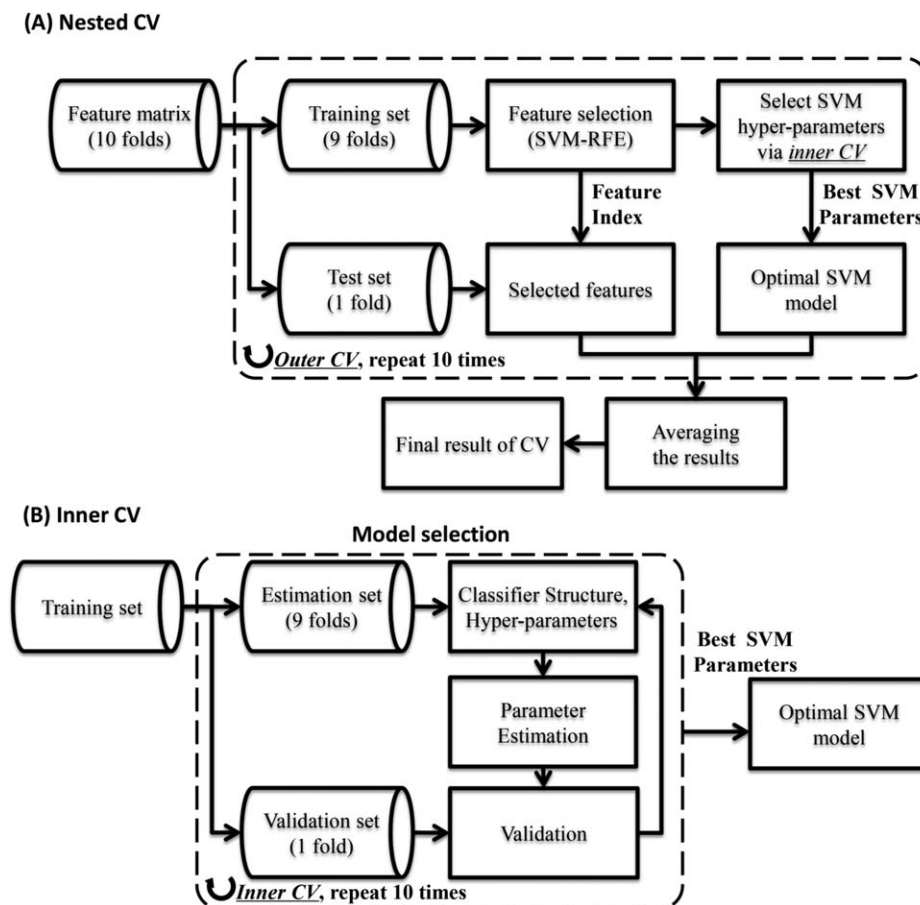


Figure 2.

The nested cross-validation strategy used in our study. **(A)** The flow chart of the nested CV strategy. The feature selection is implemented on the training set, rather than entire dataset. The performance is evaluated on independent test set in outer CV, which may avoid the overfitting problem. **(B)** The detailed

explanation of the inner CV. In the inner CV, the training set is further divided into estimation set and validation set, the SVM parameters was estimated using a grid search method on the estimation set, the validation set is used to assess the optimal SVM parameters.

estimated for each component as the proportion of permutations that yielded a larger component or one of equal size. This NBS method has recently been used to identify abnormal brain connectivity circuitry in other diseases such as ADHD [Cao et al., 2013; Hong et al., 2014] and depression [Zhang et al., 2011]. The NBS method aims to identify the connected subnetworks in the connectivity matrix that significantly differ between groups which would offer greater statistical power [Verstraete et al., 2011] and reveal more differences that probably have been overlooked with the false discovery rate (FDR) correction [Li et al., 2013].

Linking Changes to Clinical Variables

For all significantly altered nodal efficiencies in regional topological analysis, and significantly altered structural connections (SC) in NBS analysis, we examined the correlations

between these significantly altered network metrics and the clinical variables in the TS group. To lessen the concern that the between-group differences of age, gender, and head motion parameters (though all the metrics were not significantly different between groups) might significantly affect the analysis results, we performed partial correlation analyses (dependent variables: network metrics; independent variables: tic severity score/YGTSS or tics duration) using SPSS 19.0. Age, gender, and six head motion parameters (x , y , z rotation and x , y , z translation) were calculated as covariates.

Combining Complementary Network-Based Features for Individual Classification Using Multiple Kernel Learning

Apart from revealing disrupted topological properties of WM structural networks in TS using univariate approach,

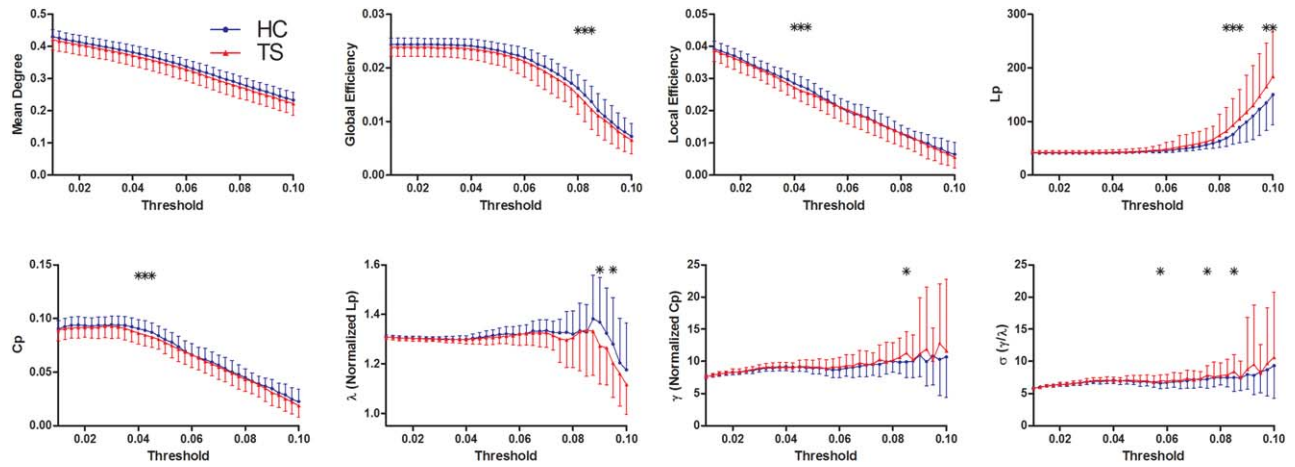


Figure 3.

Differences in topological properties of WM structural networks between TS patients and controls. Global metrics of WM structural networks were quantified in controls and TS patients with different probability thresholds. Data points marked with a star indicate a significant group difference ($P < 0.05$) in the global network metric under a corresponding threshold. Both TS patients

and controls showed a small-world organization of WM networks characterized by a $\gamma > 1$ and $\lambda \approx 1$. However, compared with controls, TS patients had significantly decreased C_p , λ , global and local efficiency, increased L_p , γ , and σ in the WM networks for a series of considered thresholds. HC, healthy controls. [Color figure can be viewed at wileyonlinelibrary.com]

we also investigate using multiple levels of network topological properties as features to accurately discriminate TS children from controls. We used the original network characteristics including 8×37 global properties (across all 37 thresholds), 90 nodal properties (AUC value), 4005 ($90 \times 89/2$) edge weights, respectively, as features for subsequent classification. As in our previous study [Wen et al., 2017a], the SVM-RFE [Guyon et al., 2002] algorithm was used for feature selection. Then, classification was performed using the support vector machine (SVM) algorithm [Cortes and Vapnik, 1995] with a radial basis function (RBF) kernel. To estimate optimal values for the two SVM parameters, the complexity or cost constant ($c > 0$) and kernel width ($\gamma > 0$), we used a grid search in the range of $c = 2^{-4}, 2^{-1}, \dots, 2^4$ and $\gamma = 2^{-8}, 2^{-9}, \dots, 2^2$, with 10-fold CV to evaluate the goodness of SVM parameters.

To further integrate the complementary information of these three kinds of network metrics (global, nodal, and edge), we employ the same multiple kernel learning (MKL) frameworks [Wen et al., 2017a] to fuse these features. The MKL algorithm can automatically search the optimal combination of the kernel matrix of these features to form an integrated kernel matrix (assigning weight to each kernel matrix), which outperforms the use of single kernels. The output of MKL is defined as

$$y_i = \sum_k \beta_k \left(\sum_j \lambda_j^k y_j K_k(x_j^k, x_i^k) \right) + b \quad (6)$$

where k denotes the k -th kind of feature; y_i denotes the corresponding class label of i -th subject; K_k is the kernel

matrix; β_k is the sub-kernel weight; λ_j^k is the Lagrange parameters; x_{jj}^k is the support vector of training set; and x_{ji}^k is the feature vector of the i -th test sample.

We used the same optimal feature subset and SVM parameters determined earlier for each single type of features (global, nodal, and edge). Our classification framework and validation experiments were implemented in Matlab using LIBSVM (v3.1.2, www.csie.ntu.edu.tw/~cjlin/libsvm/) for the SVM classifier and Shogun (v3.2.0, www.shogun-toolbox.org/) for the MKL framework.

In our study, the same nested cross-validation strategy [Wen et al., 2017a] (Fig. 2 shows the detailed flow chart) was used to evaluate the classification performance, which was considered as the excellent estimation of generalization [Wilson et al., 2009]. The statistics we used to evaluate our classification algorithm performance are accuracy, sensitivity, specificity, and the area under the curve for the receiver operated characteristic curve (AUC ROC). Accuracy is defined as $(TP + TN)/(TP + TN + FN + FP)$ where TP = true positive, TN = true negative, FP = false positive, and FN = false negative. Sensitivity is defined as $TP/(TP + FN)$ and specificity is defined as $TN/(FP + TN)$.

RESULTS

Alterations in the Global Properties of WM Networks in TS

Both TS patients and controls showed a small-world organization of WM networks characterized by $\gamma > 1$ and $\lambda \approx 1$ (Fig. 3). However, compared with controls, TS

TABLE III. Group comparisons of AUC values (%) of global network properties

	S_p	E_{glob}	E_{loc}	L_p	C_p	λ	γ	Σ
HC	3.08 ± 0.18	0.18 ± 0.01	0.2 ± 0.02	141.88 ± 8.91	0.62 ± 0.05	11.8 ± 0.28	82.78 ± 6.61	63.13 ± 4.76
TS	2.99 ± 0.3	0.17 ± 0.02	0.2 ± 0.03	135.78 ± 13.31	0.6 ± 0.07	11.68 ± 0.32	85.02 ± 11.89	65.69 ± 10.42
<i>P</i> value	0.11	0.122	0.498	0.016*	0.17	0.061	0.294	0.154

Two sample *t* tests were used to determine the differences in the global network properties between groups. AUC values (mean \pm SD) denote values of global network properties in each group.**P* < 0.05.

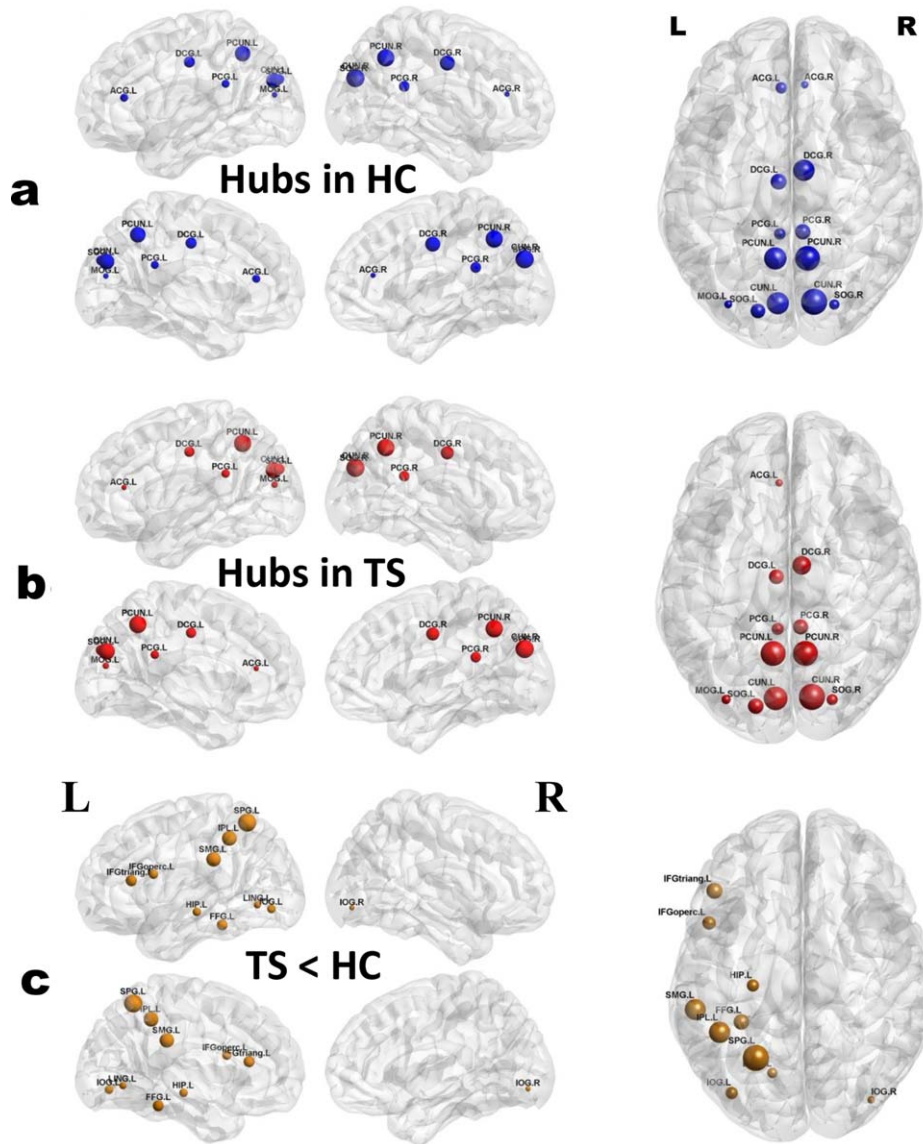


Figure 4.

Distribution of hub regions in the WM structural networks of the control and TS groups and nodes with decreased efficiency in TS children. (a,b) 3D representations of the hub distributions in the control (a) and TS (b) groups. The hub nodes are shown in blue and red with node sizes indicating their nodal efficiency values. (c) The disrupted nodes with the significant between-group differences

in the regional efficiency are shown in yellow, and the node sizes indicate the t values in t test. The brain graphs were visualized by using BrainNet Viewer software (<http://www.nitrc.org/projects/bnv/>). HC, healthy controls. For the abbreviations of nodes, see Table II. [Color figure can be viewed at wileyonlinelibrary.com]

TABLE IV. Identified hub regions of WM networks in control and TS groups

HC			TS		
Hub regions	Category	mean E_{nodal}	Hub regions	Category	mean E_{nodal}
ACG.L	Cingulate	0.215	ACG.L	Cingulate	0.211
			ACG.R	Cingulate	0.206
DCG.L	Cingulate	0.222	DCG.L	Cingulate	0.216
DCG.R	Cingulate	0.226	DCG.R	Cingulate	0.222
PCG.L	Cingulate	0.219	PCG.L	Cingulate	0.211
PCG.R	Cingulate	0.222	PCG.R	Cingulate	0.215
CUN.L	Occipital	0.232	CUN.L	Occipital	0.222
CUN.R	Occipital	0.233	CUN.R	Occipital	0.227
SOG.L	Occipital	0.223	SOG.L	Occipital	0.214
SOG.R	Occipital	0.218	SOG.R	Occipital	0.209
MOG.L	Occipital	0.216	MOG.L	Occipital	0.207
PCUN.L	Parietal	0.233	PCUN.L	Parietal	0.223
PCUN.R	Parietal	0.232	PCUN.R	Parietal	0.225

E_{nodal} represents the AUC value (%) of the nodal efficiency across thresholds.

children had significantly decreased C_p , λ , global and local efficiency, increased L_p , γ , and σ in the WM networks for different thresholds. All the significant P value (<0.05) were derived after FDR correction [Benjamini and Hochberg, 2015]. Moreover, the AUC value of the shortest path length L_p significantly increased in TS group compared to control group. There were no significant differences between groups in other network metrics (Fig. 3 and Table III).

Alterations in the Regional Properties of WM Networks in TS

We identified the hub regions of the WM networks for each group. The nodes were considered brain hubs if their nodal efficiencies (AUC value) were at least 1 standard deviation (SD) greater than the average nodal efficiency of the network.

We found that the TS and control groups showed highly similar hub distributions, with core regions mainly in the cingulate gyri (anterior, middle, and posterior part), occipital (bilateral cuneus, superior occipital gyrus, and left middle occipital gyrus), and parietal cortices (bilateral precuneus) (Fig. 4 and Table IV).

Further statistical analysis revealed that TS group had significant reduced nodal efficiency mainly in the bilateral inferior occipital gyrus and superior parietal gyrus, left lingual gyrus, left inferior frontal gyrus (opercular, triangular part), left parietal cortices (supramarginal gyrus and inferior parietal gyrus), and left temporal cortices (fusiform gyrus and hippocampus) (Table V). No node region showed significant increased nodal efficiency. Of note, the regions that showed significant reduced nodal efficiency in TS group were not the hubs regions (Fig. 4). In addition, for TS group, we found no significant correlations between nodal efficiency and clinical variables in any disrupted region.

Decreased Regional Connectivity in TS Revealed by NBS Analysis

Using the NBS analysis, two separate networks showing significantly decreased connection strengths in TS children compared with healthy children were identified (P values <0.05 , NBS corrected). The first network (network 1 in Table VI) comprised 6 links, involving 7 different brain regions, which locate in the right occipital gyrus, superior parietal gyrus, cuneus, precuneus, lingual gyrus (P values <0.05 , NBS corrected; Fig. 5). The second network (network 2 in Table VI) was composed of 4 links, involving 5 different brain regions, which locate in the left middle occipital gyrus, superior parietal gyrus, precuneus, bilateral paracentral lobule (P values <0.05 , NBS corrected; Fig. 5). The strengths, percentages, and frequencies of these decreased WM connections across thresholds are

TABLE V. Brain regions with statistically significant between-group differences in nodal efficiency

Regions	Category	E_{nodal}		P value
		HC	TS	
IFGoperc.L	Frontal	0.178 ± 0.016	0.169 ± 0.025	0.035
IFGtriang.L	Frontal	0.181 ± 0.016	0.171 ± 0.025	0.026
HIP.L	Temporal	0.159 ± 0.015	0.151 ± 0.019	0.024
LING.L	Occipital	0.191 ± 0.015	0.183 ± 0.023	0.044
IOG.L	Occipital	0.190 ± 0.015	0.180 ± 0.022	0.022
IOG.R	Occipital	0.166 ± 0.014	0.156 ± 0.020	0.012
FFG.L	Temporal	0.204 ± 0.015	0.194 ± 0.024	0.024
SPG.L	Parietal	0.195 ± 0.017	0.182 ± 0.030	0.019
SPG.R	Parietal	0.165 ± 0.019	0.154 ± 0.030	0.046
IPL.L	Parietal	0.210 ± 0.018	0.198 ± 0.031	0.041
SMG.L	Parietal	0.183 ± 0.017	0.172 ± 0.028	0.028

E_{nodal} represents the AUC values (mean ± SD) (%) of the nodal efficiency of each group.

TABLE VI. The strengths, percentages, and frequencies of decreased NBS structural connections within two separate white-matter networks across all 37 thresholds

Connection	Connection strengths		Threshold range	Percentage (frequency)
	Control	TS		
Network 1:				
Cuneus_R ↔ Occipital_Sup_R	0.177 ± 0.016	0.166 ± 0.013	0.02–0.05, 0.0575–0.6, 0.08–0.1	64.86% (24)
Occipital_Sup_R ↔ Occipital_Mid_R	0.174 ± 0.017	0.163 ± 0.019	0.02–0.05, 0.0575–0.6, 0.08–0.1	64.86% (24)
Occipital_Sup_R ↔ Parietal_Sup_R	0.064 ± 0.013	0.058 ± 0.017	0.02–0.05	35.14% (13)
Lingual_R ↔ Occipital_Inf_R	0.050 ± 0.010	0.040 ± 0.010	0.01–0.0125, 0.0575–0.6	10.81% (4)
Occipital_Mid_R ↔ Occipital_Inf_R	0.076 ± 0.011	0.066 ± 0.014	0.0575–0.6	5.41% (2)
Parietal_Sup_R ↔ Precuneus_R	0.063 ± 0.009	0.058 ± 0.014	0.05	2.70% (1)
Network 2:				
Parietal_Sup_L ↔ Precuneus_L	0.076 ± 0.011	0.069 ± 0.014	0.015–0.0175	5.41% (2)
Precuneus_L ↔ Paracentral_Lobule_L	0.042 ± 0.010	0.035 ± 0.008	0.015–0.0175	5.41% (2)
Paracentral_Lobule_L ↔ Paracentral_Lobule_R	0.031 ± 0.010	0.026 ± 0.008	0.015–0.0175	5.41% (2)
Occipital_Mid_L ↔ Parietal_Sup_L	0.030 ± 0.010	0.026 ± 0.006	0.0175	2.70% (1)

Connection strengths: mean (\pm SD) values of the connection strength (probability) in each group. Threshold range/percentage (frequency): the values represent the threshold range, the emerging percentage and times of the WM connections under all 37 thresholds (0.01–0.1, interval = 0.0025) in which the NBS components were statistically significant. For the abbreviations of the regions, see Table II.

shown in Table VI. We did not identify any network with significantly increased connectivity in the TS group. In addition, for TS group, we found no significant correlations between connection strength and clinical variables in any disrupted links.

Classification Results Using Multiple Kernel Learning

We used SVM classifier, which classifies subjects into TS group and healthy control groups. The classification accuracies of using a single type of features (global, nodal, and edge) and combining features (using MKL) are showed in Table VII. To avoid potential lack of robustness and stability of classification based on one-time random partitioning in CV, we repeated the nested CV procedure for 20 times. The highest classification performance with mean (\pm SD) accuracy ($86.47 \pm 3.71\%$), sensitivity ($85.57 \pm 4.38\%$), specificity ($87.44 \pm 4.13\%$), and ROC AUC ($92.62 \pm 3.35\%$) were achieved on the combined features using MKL, which was demonstrated to perform better than a single type of features. Figure 6A shows the receiver operating characteristic (ROC) curves of all the methods.

As the highest accuracy was achieved when combining features, the current work also identified the most discriminative network features for TS classification. As the feature selection in each fold is performed based only on the training set, the selected features could differ slightly across different cross-validation folds. Therefore, we summed the counts of each feature selected by our

proposed method over the 20 rounds nested 10-fold CV. The frequencies of the top 10 features for each type of network properties were provided in Table VIII.

For the purpose of visualization, we display the brain regions with nodal efficiencies identified as discriminative features (with frequency >0.2) for TS classification using MKL in Figure 6B.

DISCUSSION

In this study, we used probabilistic diffusion tractography and graph theory to investigate the topological organization of the WM structural networks in drug-naive TS children compared with healthy children. Both TS and healthy children showed small-world properties of the WM networks, characterized by high local clustering and short path length, which are in accordance with previous WM network studies in healthy children [Cao et al., 2013]. Despite the common small-world topology, TS children showed decreased global and local efficiency and increased shortest path length. Although both TS and control groups showed highly similar hub distributions, TS children exhibited significant decreased nodal efficiency, primarily in the inferior frontal gyrus, inferior parietal gyrus [Wittfoth et al., 2012], and hippocampus [Peterson et al., 2007], and previous studies also revealed structural alterations of these regions in TS. Furthermore, TS children exhibited decreased network connectivity, primarily in the occipital gyrus, superior parietal gyrus, cuneus, precuneus, and lingual gyrus. Finally, no significant correlation between network metrics and clinical variables was found,

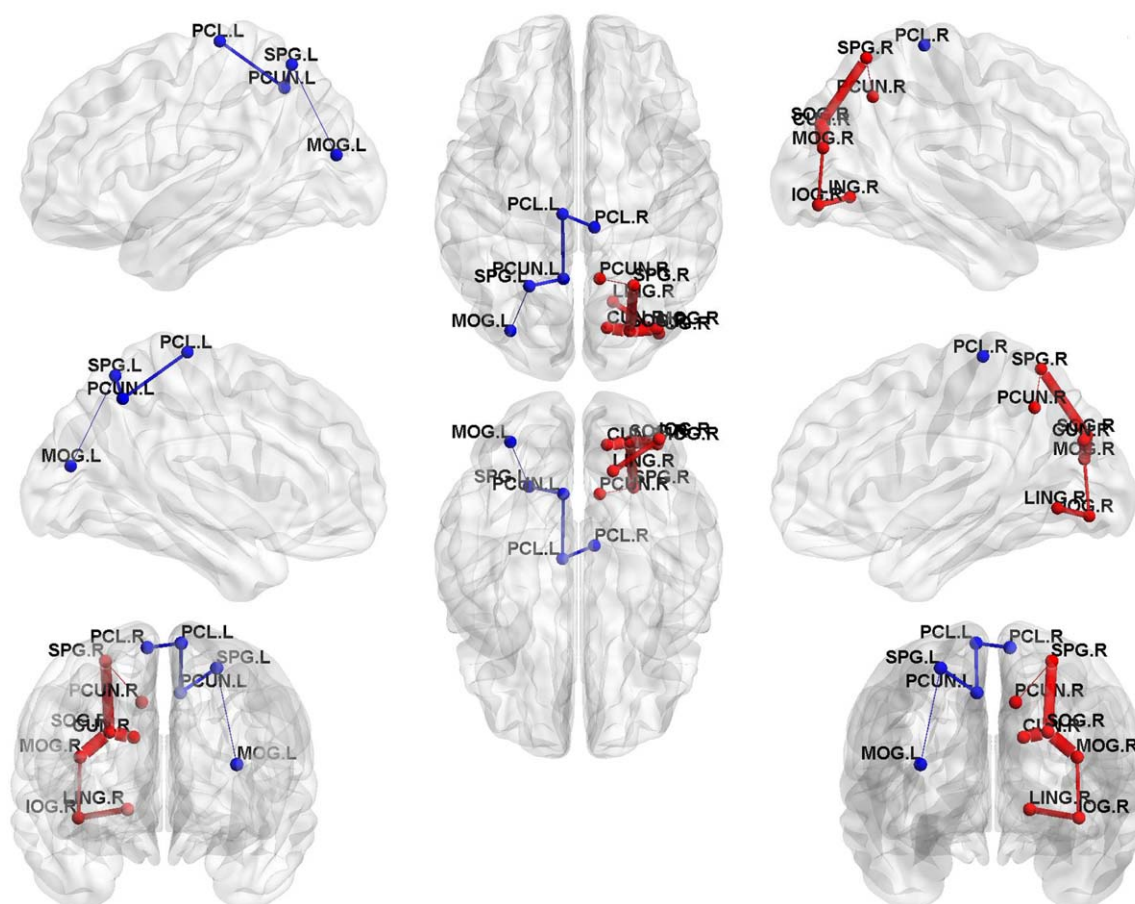


Figure 5.

Two separate networks that show decreased structural connection strengths in TS children. Two separate networks showing significantly decreased connectivity were identified in TS group compared with control group (P values < 0.05 , NBS corrected). The red nodes and edges represent network 1, primarily comprising the right parieto-occipital, precuneus, and cuneus regions. The blue nodes and edges represent network 2, involving the left parieto-occipital, precuneus, and bilateral paracentral lobule

regions. In the 3D surface view of the components, the edge widths represent the emerging percentage of the WM connections under all 37 thresholds. The nodes and connections were mapped onto the cortical surfaces using BrainNet Viewer software (<http://www.nitrc.org/projects/bnv/>). For detailed information of the WM connections in the significant NBS components, see Table VI. [Color figure can be viewed at wileyonlinelibrary.com]

using age, gender, and head motion parameters as covariates. Of note, though age is not significantly different between groups, there may still be a between-group difference ($P = 0.062$) in age. Therefore, age was calculated as a covariate to eliminate its potential impact on the correlation analysis results. Together, our study showed the disruption of topological organization in WM networks in TS children.

Altered Global Properties in the WM Networks in TS

In this study, we characterized the small-world topology of the WM networks in both TS and healthy children, using the probabilistic tractography method to map whole-brain

WM connectivity, which has advantages in tracking crossing and splitting fiber bundles compared with deterministic tractography methods [Behrens et al., 2007]. Both TS and healthy children had brain networks with small-worldness property. Small-worldness property means that the network has high efficiency in information processing and transfer [Sporns and Honey, 2006]. Previous studies have proven the small-worldness property of the brain structural network via diffusion MRI [Gong et al., 2009a; Hagmann et al., 2007; Iturria-Medina et al., 2008].

Although the structural networks in TS children showed prominent small-world topology, the global and local efficiencies were significantly decreased, while short path length and small-worldness were significantly increased at

TABLE VII. Classification performances of all methods in percentage

Feature	Accuracy (%)	Sensitivity (%)	Specificity (%)	ROC AUC (%)
Global properties	63.24 ± 3.54	64.32 ± 5.22	62.07 ± 5.57	64.09 ± 2.87
Nodal efficiencies	60.76 ± 3.82	65.11 ± 4.96	56.10 ± 7.51	62.18 ± 3.18
Pairwise SC	78.18 ± 2.82	67.95 ± 6.91	89.15 ± 3.01	88.77 ± 1.57
Combining features	86.47 ± 3.71	85.57 ± 4.38	87.44 ± 4.13	92.62 ± 3.35

a series of threshold compared with controls. The global efficiency reflects the information transfer between remote cortical regions, and it is mainly associated with long-range connections. The local efficiency is predominantly related to the short-range connections between neighboring regions. Decreases in both global and local efficiencies reflect disrupted topological organizations of the WM networks in TS patients, which could be due to impaired structural connections. Many DTI studies provided direct evidence for disrupted structural integrity in various WM tracts in TS children, such as the corticospinal tract, the superior/inferior longitudinal fasciculus, the superior/inferior fronto-occipital fasciculus, the anterior thalamic radiation, and the corpus callosum [Wen et al., 2016a]. Evidence from a magnetization transfer ratio (MTR) study also showed WM reductions in the inferior frontal gyrus and cingulate gyrus in TS patients [Muller-Vahl et al., 2009], and previous postmortem study [Thomas et al., 2004] proved MTR reductions correlate with myelin and axonal loss in the WM. So, our results showed that

reduced white matter integrity is associated with TS children [Plessen et al., 2006; Wen et al., 2016a] from a network perspective, and the reduced global and local efficiencies in TS group may indicate a disturbance of the normal balance in their structural brain network, which tends to have a more randomized configuration [Peng et al., 2014].

Moreover, significantly increased short path length and small worldness were also found for different thresholds, especially the AUC value of shortest path length was significantly increased in TS group compared to control group. Increased short path length suggests reduced efficiency of parallel information transfer in the WM networks in TS children. As the small-world connectivity model reflects an optimal balance between local specialization and global integration, the significant increased short path length and small worldness in the structural networks of TS children could indicate less optimal organization of the brain networks, possibly as a consequence of reorganization secondary to cortical injury [Liu et al., 2013a].

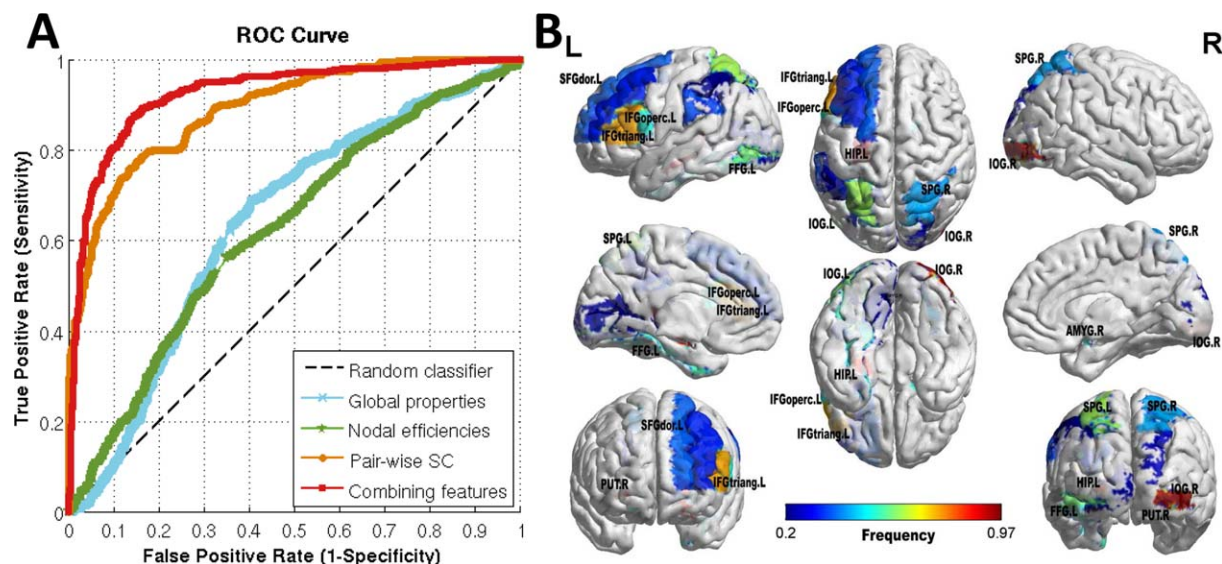


Figure 6.

Results of TS classification based on different types of features. (A) ROC curves of the classification results, which demonstrate the superior performance of using combined features over a single type of features. (B) Brain regions with nodal efficiencies identified as discriminative features for classification using MKL. The

brain graphs were visualized by *volume to surface* function in Brain-Net Viewer software. The regional colors with progressive shade (from blue to red) indicate the frequency of being selected by the nested CV procedure. Abbreviation is the same as Table II. [Color figure can be viewed at wileyonlinelibrary.com]

TABLE VIII. The top 10 features for each kind of network properties selected by the nested CV procedure as the most discriminative for TS classification

Property	Global feature		Nodal feature			Edge feature		
	Counts	Freq (%)	Region	Counts	Freq (%)	Connection	Counts	Freq (%)
λ ($T = 0.09$)*	198	99.0	IOG.R*	194	97.0	ORBinf.R-PreCG.R	200	100.0
C_p ($T = 0.045$)*	190	95.0	PUT.R	188	94.0	IFGtriang.R-MFG.R	200	100.0
σ ($T = 0.0575$)*	190	95.0	HIP.L*	175	87.5	PCG.L-INS.L	197	98.5
E_{glob} ($T = 0.085$)*	156	78.0	IFGtriang.L*	150	75.0	CUN.R-SOG.R*	192	96.0
σ ($T = 0.075$)*	155	77.5	SPG.L*	123	61.5	CUN.R-DCG.R	190	95.0
C_p ($T = 0.0425$)*	154	77.0	IOG.L*	118	59.0	DCG.R-PCG.R	189	94.5
λ ($T = 0.095$)*	136	68.0	FFG.L*	108	54.0	CAL.L-OLF.R	188	94.0
E_{loc} ($T = 0.045$)*	130	65.0	AMYG.R	107	53.5	MOG.L-SPG.L*	185	92.5
γ ($T = 0.095$)*	130	65.0	IFGperc.L*	102	51.0	SOG.R-ORBsupmed.L	185	92.5
E_{loc} ($T = 0.04$)*	128	64.0	SPG.R*	85	42.5	SOG.R-MOG.R*	184	92.0

Counts: the counts of each feature selected by our proposed method over the 20 rounds nested 10-fold CV. Freq: the frequency of being selected equals counts/total times in 20 rounds nested 10-fold CV (200 times). *Feature marked with a star (*) indicates that it was significantly altered in between-groups statistical comparison.

Highly Similar Hub Distributions Between TS and Controls

In addition to noting prominent small-world topology in both TS and healthy children, we also found that the TS and control children have highly similar hub distributions, with core regions mainly in the cingulate gyri (both anterior, middle, and posterior part), occipital (bilateral cuneus, superior occipital gyrus, left middle occipital gyrus), and parietal cortices (bilateral precuneus). Our results suggest that the key regions of structural network are conserved throughout the development process and the small-world networks can tolerate developmental alterations or disease [He et al., 2009; Supekar et al., 2009].

Of note, our results showed that the bilateral anterior, posterior cingulate gyrus, and precuneus were hub regions in both groups. These regions were in the default-mode network (DMN), one of the most described resting-state networks (RSNs). DMN activates when an individual is awake and alert, but is not actively involved in an attention demanding or goal-directed task. Although the DMN concept is derived from resting-state functional MRI, some recent studies have combined fMRI and DTI in healthy participants [Greicius et al., 2009; Horn et al., 2014; Oort et al., 2013; Supekar et al., 2010], reporting significant correlations between the DMN structural and functional connections. A previous WM network study also showed similar hubs regions within DMN in healthy children [Cao et al., 2013] as ours. In particular, bilateral precuneus with DMN were found to be consistent rich-club hub regions in both TS and healthy children [Wen et al., 2017c]. Our finding of highly similar hub distributions between groups is also largely consistent with this study.

Distributed Regions With Altered Efficiency in TS

In this study, we observed several brain regions with reduced efficiency in TS children, primarily in the occipital

gyrus (bilateral inferior occipital gyrus, left ingual gyrus), left inferior frontal gyrus (opercular, triangular part), left parietal (supramarginal gyrus, superior and inferior parietal gyrus), and left temporal cortices (fusiform gyrus and hippocampus). These regions are key nodes in the brain networks and exhibit structural and functional abnormalities in TS [Wen et al., 2016a; Wen et al., 2017d], which were involved in visual, default-mode, language, and sensorimotor-related areas.

First, reduced nodal efficiencies were also found in several occipital regions (inferior occipital gyrus and lingual gyrus) that are important for visual processing. Few studies have identified structural abnormalities in the TS patients in the visual regions. Smaller inferior occipital volumes were found in TS subjects [Peterson et al., 2001] and WM volumes decreased in left lingual gyrus [Liu et al., 2013b]. Of note, the nodal efficiency of right inferior occipital gyrus was also reported to be one of the discriminative structural network features for differentiating early TS children from healthy children [Wen et al., 2016b]. Despite these advances, very little is known about the alterations in the topological organization of network in visual regions. Thus, our results provide further evidence for the structural disruption of the visual system in TS patients.

Second, we observed a decreased nodal efficiency in the structural networks of TS children in several default-mode regions (hippocampus and inferior parietal lobules). These regions represent core components of the DMN, which has been reported to be highly related to tic generation in adult TS patients [Neuner et al., 2014]. Cui et al. [2014] found that TS children showed significantly decreased ALFF in the inferior parietal lobules (IPL). Furthermore, functional abnormalities in the IPL have been described before [Swick et al., 2011]. Hippocampal volume alterations were also been found in TS boys and structural changes in hippocampus might indicate an involvement of

temporolimbic pathways of the CSTC in the syndrome [Ludolph et al., 2006]. Previous studies combined DTI tractography with resting-state functional connectivity MRI to demonstrate that resting-state functional connectivity could reflect structural connectivity in the DMN [Greicius et al., 2009]. Thus, our results are in agreement with these previous findings.

Third, reduced nodal efficiencies were observed in several frontal regions (IFG_{operc}, IFG_{triang}) that are key components for language processing. The IFG_{operc} and IFG_{triang}, comprising Broca's area, especially in the left hemisphere, are known to be important for language synthesis. Structural and functional changes in the inferior frontal gyrus (IFG) regions in TS patients have been reported in previous neuroimaging studies [Ganos et al., 2014; Wittfoth et al., 2012]. Apart from playing a key role in tic inhibition [Ganos et al., 2014], the left IFG has also been associated with aspects of language processing [Liakakis et al., 2011]. Particularly, several previous studies have indicated that the left IFG (e.g., IFG_{operc.L} and IFG_{triang.L}) are important for elaborated semantic inhibition [Zhu et al., 2009, 2013]. In this study, 28 of 44 TS patients exhibited vocal tic (including humming, grunting, or saying actual words, usually in an explosive fashion and the words may involve curses), which supports our findings of the abnormalities in the language areas.

Finally, we observed reduced nodal efficiencies in the bilateral superior parietal lobe, which is related to sensorimotor association functions. A previous study [Wolpert et al., 1998] suggests that the superior parietal lobe is critical for sensorimotor integration, by maintaining an internal representation of the body's state. Buse et al. [2015] found decreased prepulse inhibition related BOLD activity in TS boys in the superior parietal cortex. Bohlhalter et al. [2006] showed that at the beginning of tic action, significant fMRI activities were found in sensorimotor areas including the superior parietal lobule bilaterally and cerebellum. Morphological studies also reported increases in GM volumes in left superior parietal lobule [Liu et al., 2011] or cortical GM volumes in superior parietal lobule showing significant correlations with clinical scores [Wittfoth et al., 2012]. These findings suggest that structural and functional changes exist in the sensorimotor-related areas in patients with TS, which provides support for our findings.

Of note, many TS children were reported to also have fine motor control and visual-motor integration impairment. A neuropsychological model of visual-motor integration skill was proposed and tested in 50 TS children and 23 unaffected age-matched control children [Schultz et al., 1998], which suggests that the integration of visual inputs and organized motor output is a specific area of neuropsychological weakness among TS children. Our studies revealed regional efficiencies decreased in visual- and motor-related areas in TS children. This finding reflects a less optimal balance between local specialization and global visual-motor integration in structural networks,

which may weaken visual-motor integration functioning in TS children.

Decreased Connectivity of Parieto-Occipital Association Areas in TS

We observed aberrant structural connectivity in two networks in TS patients. One network with decreased connection strengths was primarily composed of the bilateral occipital gyrus, superior parietal gyrus, and right cuneus. Decreased structural connectivity means biologically the decreased WM connection probabilistic between regions, and decreased WM connection probability or fractional anisotropy (FA) values are usually associated with disease pathology [Cao et al., 2013]. Superior occipital gyrus follows the superior edge of the lobe and merges with cuneus on the medial surface of the occipital lobe, and this link connecting the superior occipital gyrus to the cuneus showed the significantly decreased structural connection strength in NBS analysis. At the level of the parieto-occipital fissure, the superior parietal gyrus is linked to the superior occipital gyrus by a transitional area called arcus parieto-occipitalis, and this link also showed significantly decreased structural connection strength.

Previous studies using structural MRI in TS provided some evidence for parieto-occipital anatomical abnormalities. TS children (5–18 years) were found to have larger cortical volumes in parieto-occipital regions [Peterson et al., 2001] compared to unaffected children, which also suggest a possible connection that increased volumes of parieto-occipital cortex are significantly correlated with tic severity. However, at present, it is unclear whether, or how, larger parieto-occipital volumes in TS children affect the abnormal structural connectivity in those regions. In addition to volumetric approaches, DTI has also been used to investigate, indirectly, the microstructural properties of the regions in TS. The previous diffusion MRI studies found decreased FA and increased MD in superficial WM regions of parieto-occipital cortex in TS children [Wen et al., 2016a] and suggested that a disrupted myelination mechanism underlie the abnormalities. Increased MD value or decreased FA values could reflect reduced myelination, fewer axons, or atypical organization of axons within the WM tract. Considering the somewhat consistent finding of increased cortical volumes, increased MD value, or decreased FA value in TS children, those microstructural differences would likely coincide with altered cortical volumes. Our study made a meaningful exploration of this issue, providing interesting and potentially valuable information about the regional morphology, WM properties and whole-brain structural networks in TS children.

Decreased Connectivity of Precuneus, Paracentral Lobule in TS

The second network component with decreased WM connections in TS primarily involved the precuneus and

paracentral lobule. As the precuneus is a part of the superior parietal lobule forward of the occipital lobe (cuneus), the precuneus linking the superior parietal gyrus and paracentral lobule were two important connections with significantly decreased connectivity in our study. The precuneus has been suggested to be the hub of the DMN that is activated during “resting consciousness” in which people do not engage intentionally in sensory or motor activity [Cavanna, 2007]. Bullmore et al. also proposed that its functions link to its role as a central and well connected “small-world network” hub between parietal and prefrontal regions [Bullmore and Sporns, 2009]. Furthermore, our result showed that the precuneus is also a structural hub and its structural connection with parietal regions is significantly disrupted in TS children. The previous study [Wen et al., 2016a] also reported significantly reduced FA value or increased RD value in precuneus WM, which reveals microstructural abnormalities in this region and is in line with our finding.

Of note, the precuneus, inferior parietal gyrus (IPL), median cingulate (DCG), and frontal cortex are key components in the “frontoparietal” network. A previous study [Church et al., 2009] revealed that pediatric TS patients showed immature and anomalous patterns of functional connectivity, primarily in the frontoparietal network, which is important for online adaptive control. Our results also revealed regional efficiencies decrease in the IPL and frontal cortex. The disrupted structural connectivity in frontoparietal network may lead the functional underconnectivity [Church et al., 2009], which could affect the communication and coordination of activity between the cerebellum, frontal cortex, and parietal cortex, related to distinctive symptoms in different developmental disorders. Furthermore, a previous WM structural networks study [Wen et al., 2017b] also found that the nodal topological properties of precuneus and paracentral lobule were discriminative features for TS classification, which could be used as biomarkers for TS pathology.

The MKL Framework Combining Complementary Network-Based Features Has Stronger Classifying Ability

Identification of objective neuroimaging biomarkers is of great interest as it could, ultimately, assist clinical decisions for individual patients. To date, TS diagnosis mainly depends on the qualitative description of symptoms as there is no hallmark imaging abnormality in routine examination or other reliable diagnostic biomarkers [Felling and Singer, 2011]. Specially, network-based biomarkers can capture the role of brain network structure in a phenotype and study the role of known subsystems for a given disorder, thereby defining new potential beneficial neuroimaging biomarkers. With this consideration, a previous study [Greene et al., 2016] used resting-state functional

connectivity (RSFC) MRI to construct the RSFC networks by calculating the correlation (r value) of each ROI’s time-course with every other ROI’s time-course. The functional connections (r value) were directly regarded as features and fed into SVM for distinguishing TS children from healthy children. The peak accuracy reached 74% with sensitivity of 76% and specificity of 71%. Nevertheless, as the human brain is a very complex and rich network, solely relying on low-level original connectivity values as features cannot capture high-level topological properties of this network. In addition, the conventional single-kernel SVM used for classification cannot optimize kernel weights of different types of features, therefore, cannot reflect the different discriminative ability of features for classification.

In this study, we combined multiple levels of original topological properties of WM structural networks, and then used the MKL framework to fuse the complementary network-based features. We implemented feature selection algorithm on the original features without between-group statistical comparison to select significantly altered features first, which can ensure SVM results have good generalization ability as in our previous study [Wen et al., 2017a]. The classification performances with higher accuracy, sensitivity, and specificity in our study than the previous study [Greene et al., 2016] have shown that the integration of multiple kernels not only increases the classification accuracy but also enhances the interpretability of the results. For each feature, we also counted its selection frequency by SVM-RFE method in nested CV procedure, to reveal the discriminative features for classification. Our results showed that the features with significant between-group difference might differ from the features that were highly discriminative in distinguishing two groups. Therefore, we combined between-group statistical comparison and SVM based individual classification to provide complementary information for assisting clinical TS diagnosis.

CONCLUSION

In this study, we used probabilistic diffusion tractography and graph theoretical analyses to investigate TS-related changes in the topological organization of WM structural networks. We found that, compared with healthy children, despite TS children showed small-world property, they had a reduced network efficiency in their brain networks, with the most pronounced reduction observed in the visual, default-mode, language, and sensorimotor association regions. In addition, two separate network components showing significantly decreased connection strengths were identified by NBS analysis, primarily composed of the parieto-occipital cortex, precuneus, and paracentral lobule. Importantly, to enhance our contributions to clinical application, we employed the MK-SVM frameworks to fuse multiple levels of network topological properties as features for accurate classification of

individuals, achieving high accuracy of 86.47%. Together, our results suggest a disrupted integrity in the large-scale brain systems in TS and provide structural insights into the brain networks of TS children. This study may extend our understanding of how structural disruptions of neuronal circuits link to the pathophysiology of TS. The most discriminative network topological features for classification will be potential quantitative neuroimaging biomarkers for assisting the clinical TS diagnosis.

ACKNOWLEDGMENT

The authors thank Dr Hao Huang at University of Pennsylvania for consultation and support on MR pulse sequences.

REFERENCES

- Basser PJ, Mattiello J, LeBihan D (1994a): Estimation of the effective self-diffusion tensor from the NMR spin echo. *J Magn Reson Ser B* 103:247–254.
- Basser PJ, Mattiello J, LeBihan D (1994b): MR diffusion tensor spectroscopy and imaging. *Biophys J* 66:259–267.
- Basser PJ, Pajevic S, Pierpaoli C, Duda J, Aldroubi A (2000): In vivo fiber tractography using DT-MRI data. *Magn Reson Med* 44:625–632.
- Behrens TE, Berg HJ, Jbabdi S, Rushworth MF, Woolrich MW (2007): Probabilistic diffusion tractography with multiple fibre orientations: What can we gain? *NeuroImage* 34:144–155.
- Benjamini Y, Hochberg Y (2015): Controlling the false discovery rate - A practical and powerful approach to multiple testing. *J R Stat Soc* 57:289–300.
- Bohlhalter S, Goldfine A, Matteson S, Garraux G, Hanakawa T, Kansaku K, Wurzman R, Hallett M (2006): Neural correlates of tic generation in Tourette syndrome: An event-related functional MRI study. *Brain* 129:2029–2037.
- Bullmore E, Sporns O (2009): Complex brain networks: Graph theoretical analysis of structural and functional systems. *Nat Rev Neurosci* 10:186–198.
- Buse J, Beste C, Herrmann E, Roessner V (2015): Neural correlates of altered sensorimotor gating in boys with Tourette Syndrome: A combined EMG/fMRI study. *World J Biol Psychiatry* 1–11.
- Cao Q, Shu N, An L, Wang P, Sun L, Xia MR, Wang JH, Gong GL, Zang YF, Wang YF, He Y (2013): Probabilistic diffusion tractography and graph theory analysis reveal abnormal white matter structural connectivity networks in drug-naive boys with attention deficit/hyperactivity disorder. *J Neurosci* 33:10676–10687.
- Cavanna AE (2007): The precuneus and consciousness. *CNS Spectr* 12:545–552.
- Cavanna AE, Seri S (2013): Tourette's syndrome. *BMJ* 347:67–71.
- Chen YF (2002): Chinese classification of mental disorders (CCMD-3): Towards integration in international classification. *Psychopathology* 35:171.
- Cheng B, Braass H, Ganos C, Treszl A, Biermann-Ruben K, Hummel FC, Muller-Vahl K, Schnitzler A, Gerloff C, Munchau A, Thomalla G (2014): Altered intrahemispheric structural connectivity in Gilles de la Tourette syndrome. *NeuroImage Clin* 4:174–181.
- Cherine F, Uicheul Y, Samir D, Oliver L, John C, Rozie A, Guy R, Paul S, Kirk F, Catherine B (2010): Somatosensory-motor bodily representation cortical thinning in Tourette: Effects of tic severity, age and gender. *Cortex* 46:750–760.
- Church JA, Fair DA, Dosenbach NUF, Cohen AL, Miezin FM, Petersen SE, Schlaggar BL (2009): Control networks in paediatric Tourette syndrome show immature and anomalous patterns of functional connectivity. *Brain* 132:225–238.
- Cortes C, Vapnik V (1995): Support-vector networks. *Mach Learn* 20:273–297.
- Cui Y, Jin Z, Chen X, He Y, Liang X, Zheng Y (2014): Abnormal baseline brain activity in drug-naive patients with Tourette syndrome: A resting-state fMRI study. *Front Hum Neurosci* 7:913.
- Dai D, He H, Vogelstein JT, Hou Z (2013): Accurate prediction of AD patients using cortical thickness networks. *Mach Vis Appl* 24:1445–1457.
- Dai D, Wang J, Hua J, He H (2012): Classification of ADHD children through multimodal Magnetic Resonance Imaging. *Front Syst Neurosci* 6:63–63.
- Felling RJ, Singer HS (2011): Neurobiology of tourette syndrome: Current status and need for further investigation. *J Neurosci* 31:12387–12395.
- Ganos C, Kahl U, Brandt V, Schunke O, Baumer T, Thomalla G, Roessner V, Haggard P, Munchau A, Kuhn S (2014): The neural correlates of tic inhibition in Gilles de la Tourette syndrome. *Neuropsychologia* 65:297–301.
- Golden GS (1977): The effect of central nervous system stimulants on Tourette syndrome. *Ann Neurol* 2:69–70.
- Gong G, He Y, Concha L, Lebel C, Gross DW, Evans AC, Beaulieu C (2009a): Mapping anatomical connectivity patterns of human cerebral cortex using in vivo diffusion tensor imaging tractography. *Cereb Cortex* 19:524–536.
- Gong G, Rosa-Neto P, Carbonell F, Chen ZJ, He Y, Evans AC (2009b): Age- and gender-related differences in the cortical anatomical network. *J Neurosci* 29:15684–15693.
- Greene DJ, Church JA, Dosenbach NUF, Nielsen AN, Adeyemo B, Nardos B, Petersen SE, Black KJ, Schlaggar BL (2016): Multivariate pattern classification of pediatric Tourette syndrome using functional connectivity MRI. *Dev Sci*.
- Greicius MD, Kaustubh S, Vinod M, Dougherty RF (2009): Resting-state functional connectivity reflects structural connectivity in the default mode network. *Cereb Cortex* 19:72–78.
- Guyon I, Weston J, Barnhill S, Vapnik V (2002): Gene selection for cancer classification using support vector machines. *Mach Learn* 46:389–422.
- Hagmann P, Kurrant M, Gigandet X, Thiran P, Wedeen VJ, Meuli R, Thiran JP (2007): Mapping human whole-brain structural networks with diffusion MRI. *Plos One* 2:e597.
- He Y, Dagher A, Chen Z, Charil A, Zijdenbos A, Worsley K, Evans A (2009): Impaired small-world efficiency in structural cortical networks in multiple sclerosis associated with white matter lesion load. *Brain* 132:3366–3379.
- Hong SB, Zalesky A, Fornito A, Park S, Yang YH, Park MH, Song IC, Sohn CH, Shin MS, Kim BN, Cho SC, Han DH, Cheong JH, Kim JW (2014): Connectomic disturbances in attention-deficit/hyperactivity disorder: A whole-brain tractography analysis. *Biol Psychiatry* 76:656–663.
- Horn A, Ostwald D, Reisert M, Blankenburg F (2014): The structural-functional connectome and the default mode network of the human brain. *NeuroImage* 102 Pt 1:142–151.

- Humphries MD, Prescott TJ (2006): The brainstem reticular formation is a small-world, not scale-free, network. *Proc R Soc B Biol Sci* 273:503–511.
- Iturria-Medina Y, Sotero RC, Canales-Rodriguez EJ, Aleman-Gomez Y, Melie-Garcia L (2008): Studying the human brain anatomical network via diffusion-weighted MRI and Graph Theory. *NeuroImage* 40:1064–1076.
- Jie B, Zhang D, Gao W, Wang Q, Wee CY, Shen D (2014): Integration of network topological and connectivity properties for neuroimaging classification. *IEEE Trans Biomed Eng* 61: 576–589.
- Jin Y, Wee CY, Shi F, Thung KH, Ni D, Yap PT, Shen D (2015): Identification of infants at high-risk for autism spectrum disorder using multiparameter multiscale white matter connectivity networks. *Hum Brain Mapp*.
- Leckman JF, Riddle MA, Hardin MT, Ort SI, Swartz KL, Stevenson J, Cohen DJ (1989): The Yale Global Tic Severity Scale: Initial testing of a clinician-rated scale of tic severity. *J Am Acad Child Adolesc Psychiatry* 28:566–573.
- Li Y, Jewells V, Kim M, Chen Y, Moon A, Armao D, Troiani L, Markovic-Plese S, Lin W, Shen D (2013): Diffusion tensor imaging based network analysis detects alterations of neuroconnectivity in patients with clinically early relapsing-remitting multiple sclerosis. *Hum Brain Mapp* 34: 3376–3391.
- Liakakis G, Nickel J, Seitz RJ (2011): Diversity of the inferior frontal gyrus—a meta-analysis of neuroimaging studies. *Behav Brain Res* 225:341–347.
- Liu Y, Peng Y, Gao P, Nie B (2011): Volume changes of whole brain gray and white matter in children patients with Tourette’s syndrome: Evidence from voxel-based morphometry. *Pediatric Res* 70:187–187.
- Liu Y, Duan YY, He Y, Wang J, Xia MR, Yu CS, Dong HQ, Ye J, Butzkueven H, Li KC, Shu N (2013a): Altered topological organization of white matter structural networks in patients with neuromyelitis optica. *Mult Scler J* 19:666–667.
- Liu Y, Miao W, Wang J, Gao P, Yin G, Zhang L, Lv C, Ji Z, Yu T, Sabel BA, He H, Peng Y (2013b): Structural abnormalities in early Tourette syndrome children: A combined voxel-based morphometry and tract-based spatial statistics study. *Plos One* 8:e76105.
- Liu F, Wee CY, Chen H, Shen D (2014): Inter-modality relationship constrained multi-modality multi-task feature selection for Alzheimer’s Disease and mild cognitive impairment identification. *NeuroImage* 84:466–475.
- Lo CY, Wang PN, Chou KH, Wang J, He Y, Lin CP (2010): Diffusion tensor tractography reveals abnormal topological organization in structural cortical networks in Alzheimer’s disease. *J Neurosci* 30:16876–16885.
- Ludolph AG, Juengling FD, Libal G, Ludolph AC, Fegert JM, Kassubek J (2006): Grey-matter abnormalities in boys with Tourette syndrome: Magnetic resonance imaging study using optimised voxel-based morphometry. *Br J Psychiatry* 188: 484–485.
- Müller-Vahl KR, Grosskreutz J, Prell T, Kaufmann J, Bodammer N, Peschel T (2014): Tics are caused by alterations in prefrontal areas, thalamus and putamen, while changes in the cingulate gyrus reflect secondary compensatory mechanisms. *BMC Neurosci* 15:65–70.
- Makki MI, Behen M, Bhatt A, Wilson B, Chugani HT (2008): Microstructural abnormalities of striatum and thalamus in children with Tourette syndrome. *Movement Disord* 23:2349–2356.
- Marques P, Soares JM, Magalhaes R, Santos NC, Sousa N (2015): The bounds of education in the human brain connectome. *Sci Rep* 5:12812.
- Maslov S, Sneppen K (2002): Specificity and stability in topology of protein networks. *Science* 296:910–913.
- Miller AM, Ravi B, Xuejun H, Juan Pablo SP, Sobel LJ, Jun L, Dongrong X, Hongtu Z, M Mallar C, Kathleen D (2010): Enlargement of thalamic nuclei in Tourette syndrome. *Arch Gen Psychiatry* 67:955.
- Mink JW (2003): The basal ganglia and involuntary movements: Impaired inhibition of competing motor patterns. *Arch Neurol* 60:1365–1368.
- Muller-Vahl KR, Kaufmann J, Grosskreutz J, Dengler R, Emrich HM, Peschel T (2009): Prefrontal and anterior cingulate cortex abnormalities in Tourette Syndrome: Evidence from voxel-based morphometry and magnetization transfer imaging. *BMC Neurosci* 10:47.
- Neuner I, Kupriyanova Y, Stocker T, Huang R, Posnansky O, Schneider F, Tittgemeyer M, Shah NJ (2010): White-matter abnormalities in Tourette syndrome extend beyond motor pathways. *NeuroImage* 51:1184–1193.
- Neuner I, Kupriyanova Y, Stocker T, Huang RW, Posnansky O, Schneider F, Shah NJ (2011): Microstructure assessment of grey matter nuclei in adult tourette patients by diffusion tensor imaging. *Neurosci Lett* 487:22–26.
- Neuner I, Werner CJ, Arrubla J, Stöcker T, Ehlen C, Wegener HP, Schneider F, Shah NJ (2014): Imaging the where and when of tic generation and resting state networks in adult Tourette patients. *Front Hum Neurosci* 8:67–77.
- Oort ESBV, Walsum AMVCV, Norris DG (2013): An investigation into the functional and structural connectivity of the Default Mode Network. *NeuroImage* 90:381–389.
- Parker CS, Deligianni F, Cardoso MJ, Daga P, Modat M, Dayan M, Clark CA, Ourselin S, Clayden JD (2014): Consensus between pipelines in structural brain networks. *Plos One* 9: e111262-e111262.
- Peng Z, Shi F, Shi C, Yang Q, Chan RC, Shen D (2014): Disrupted cortical network as a vulnerability marker for obsessive-compulsive disorder. *Brain Struct Funct* 219: 1801–1812.
- Peterson BS, Choi HA, Hao X, Amat JA, Zhu H, Whiteman R, Liu J, Xu D, Bansal R (2007): Morphologic features of the amygdala and hippocampus in children and adults with Tourette syndrome. *Arch Gen Psychiatry* 64:1281–1291.
- Peterson BS, Staib L, Scahill L, Zhang H, Anderson C, Leckman JF, Cohen DJ, Gore JC, Albert J, Webster R (2001): Regional brain and ventricular volumes in Tourette syndrome. *Arch Gen Psychiatry* 58:427–440.
- Peterson BS, Thomas P, Kane MJ, Scahill L, Zhang HP, Bronen R, King RA, Leckman JF, Staib L (2003): Basal ganglia volumes in patients with Gilles de la Tourette syndrome. *Arch Gen Psychiatry* 60:415–424.
- Plessen KJ, Gruner R, Lundervold A, Hirsch JG, Xu D, Bansal R, Hammar A, Lundervold AJ, Wentzel-Larsen T, Lie SA, Gass A, Peterson BS, Hugdahl K (2006): Reduced white matter connectivity in the corpus callosum of children with Tourette syndrome. *J Child Psychol Psychiatry Allied Discip* 47: 1013–1022.
- Plessen KJ, Wentzel-Larsen T, Hugdahl K, Feineigle P, Klein J, Staib LH, Leckman JF, Bansal R, Peterson BS (2004): Altered interhemispheric connectivity in individuals with Tourette’s disorder. *Am J Psychiatry* 161:2028–2037.

- Qi S, Meesters S, Nicolay K, Bm THR, Ossenblok P (2016): Structural brain network: What is the effect of LiFE optimization of whole brain tractography? *Front Comput Neurosci* 10:
- Retz-Junginger P, Retz W, Blocher D, Stieglitz RD, Georg T, Supprian T, Wender PH, Rosler M (2003): Reliability and validity of the Wender-Utah-Rating-Scale short form. Retrospective assessment of symptoms for attention deficit/hyperactivity disorder. *Der Nervenarzt* 74:987–993.
- Robertson WC, Kao A (2011): Tourette syndrome and other Tic disorders. Medscape
- Sacchet MD, Prasad G, Folandross LC, Thompson PM, Gotlib IH (2015): Support vector machine classification of major depressive disorder using diffusion-weighted neuroimaging and graph theory. *Front Psychiatry* 6:21.
- Scahill L, Riddle MA, McSwiggin-Hardin M, Ort SI, King RA, Goodman WK, Cicchetti D, Leckman JF (1997): Children's Yale-Brown obsessive compulsive scale: Reliability and validity. *J Am Acad Child Adolesc Psychiatry* 36:844–852.
- Schultz RT, Carter AS, Gladstone M, Scahill L, Leckman JF, Peterson BS, Zhang H, Cohen DJ, Pauls D (1998): Visual-motor integration functioning in children with Tourette syndrome. *Neuropsychology* 12:134–145.
- Shu N, Liu Y, Li K, Duan Y, Wang J, Yu C, Dong H, Ye J, He Y (2011): Diffusion tensor tractography reveals disrupted topological efficiency in white matter structural networks in multiple sclerosis. *Cereb Cortex* 21:2565–2577.
- Sowell E, Kan EJ, Thompson P, Bansal R, Xu D, Toga A, Peterson B (2008): Thinning of sensorimotor cortices in children with Tourette syndrome. *Nat Neurosci* 11:637–639.
- Sporns O, Honey CJ (2006): Small worlds inside big brains. *Proc Natl Acad Sci USA* 103:19219–19220.
- Sporns O, Tononi G, Kötter R (2005): The human connectome: A structural description of the human brain. *PLoS Comput Biol* 1:e42.
- Stokes A, Bawden HN, Camfield PR, Backman JE, Dooley JM (1991): Peer problems in Tourettes disorder. *Pediatrics* 87:936–942.
- Supekar K, Musen M, Menon V (2009): Development of large-scale functional brain networks in children. *PLoS Biol* 7:e1000157.
- Supekar K, Uddin LQ, Prater K, Amin H, Greicius MD, Menon V (2010): Development of functional and structural connectivity within the default mode network in young children. *NeuroImage* 52:290–301.
- Swick D, Ashley V, Turken U (2011): Are the neural correlates of stopping and not going identical? Quantitative meta-analysis of two response inhibition tasks. *NeuroImage* 56:1655–1665.
- Telesford QK, Joyce KE, Hayasaka S, Burdette JH, Laurienti PJ (2011): The ubiquity of small-world networks. *Brain Connect* 1:367–375.
- Thomas E, Michael S, Joern K, Christoph S, Thomas P, Nils B, Hans Jochen H, Mircea Ariel S (2004): Differentiation of idiopathic Parkinson's disease, multiple system atrophy, progressive supranuclear palsy, and healthy controls using magnetization transfer imaging. *NeuroImage* 21:229–235.
- Tzourio-Mazoyer N, Landeau B, Papathanassiou D, Crivello F, Etard O, Delcroix N, Mazoyer B, Joliot M (2002): Automated anatomical labeling of activations in SPM using a macroscopic anatomical parcellation of the MNI MRI single-subject brain. *NeuroImage* 15:273–289.
- van den Heuvel MP, Mandl RC, Stam CJ, Kahn RS, Hulshoff Pol HE (2010): Aberrant frontal and temporal complex network structure in schizophrenia: A graph theoretical analysis. *J Neurosci* 30:15915–15926.
- Verstraete E, Veldink JH, Mandl RC, van den Berg LH, van den Heuvel MP (2011): Impaired structural motor connectome in amyotrophic lateral sclerosis. *Plos One* 6:e24239.
- Watts DJ, Strogatz SH (1998): Collective dynamics of 'small-world' networks. *Nature* 393:440–442.
- Wen H, Liu Y, Wang J, Rekik I, Zhang J, Zhang Y, Tian H, Peng Y, He H (2016a): Combining tract- and atlas-based analysis reveals microstructural abnormalities in early Tourette syndrome children. *Hum Brain Mapp* 37:1903–1919.
- Wen H, Liu Y, Wang J, Zhang J, Peng Y, He H (2016b): A Diagnosis Model for Early Tourette Syndrome Children Based on Brain Structural Network Characteristics. *International Society for Optics and Photonics*. p 97852R-97852R-9.
- Wen H, Liu Y, Rekik I, Wang S, Chen Z, Zhang J, Zhang Y, Peng Y, He H (2017a): Multi-modal multiple kernel learning for accurate identification of Tourette syndrome children. *Pattern Recogn* 63:601–611.
- Wen H, Liu Y, Wang S, Li Z, Zhang J, Peng Y, He H (2017b): Multi-threshold white matter structural networks fusion for accurate diagnosis of early Tourette syndrome children. *International Society for Optics and Photonics*. p 101341Q-101341Q-13.
- Wen H, Liu Y, Wang S, Zhang J, Peng Y, He H (2017c): Diffusion Tractography and Graph Theory Analysis Reveal the Disrupted Rich-Club Organization of White Matter Structural Networks in Early Tourette Syndrome Children. *International Society for Optics and Photonics*. p 101371E-101371E-12.
- Wen H, Liu Y, Rekik I, Wang S, Chen Z, Zhang J, Zhang Y, Peng Y, He H (2017d): Combining Disrupted and Discriminative Topological Properties of Functional Connectivity Networks as Neuroimaging Biomarkers for Accurate Diagnosis of Early Tourette Syndrome Children.
- Werner CJ, Stöcker T, Kellermann T, Bath J, Beldoch M, Schneider F, Wegener HP, Shah JN, Neuner I (2011): Altered motor network activation and functional connectivity in adult tourette's syndrome. *Hum Brain Mapp* 32:2014–2026.
- Wilson SM, Ogar JM, Laluz V, Growdon M, Jang J, Glenn S, Miller BL, Weiner MW, Gorno-Tempini ML (2009): Automated MRI-based classification of primary progressive aphasia variants. *NeuroImage* 47:1558–1567.
- Wittfoth M, Bornmann S, Peschel T, Grosskreutz J, Glahn A, Buddensiek N, Becker H, Dengler R, Müller-Vahl KR (2012): Lateral frontal cortex volume reduction in Tourette syndrome revealed by VBM. *BMC Neurosci* 13:17.
- Wolpert DM, Goodbody SJ, Husain M (1998): Maintaining internal representations: The role of the human superior parietal lobe. *Nat Neurosci* 1:529–533.
- Worbe Y, Malherbe C, Hartmann A, Pelegrini-Issac M, Messe A, Vidailhet M, Lehericy S, Benali H (2012): Functional immaturity of cortico-basal ganglia networks in Gilles de la Tourette syndrome. *Brain* 135:1937–1946.
- Worbe Y, Marrakchi-Kacem L, Lecomte S, Valabregue R, Poupon F, Guevara P, Tucholka A, Mangin JF, Vidailhet M, Lehericy S, Hartmann A, Poupon C (2015): Altered structural connectivity of cortico-striato-pallido-thalamic networks in Gilles de la Tourette syndrome. *Brain* 138:472–482.
- Yendiki A, Koldewyn K, Kakunoori S, Kanwisher N, Fischl B (2014): Spurious group differences due to head motion in a diffusion MRI study. *NeuroImage* 88:79–90.
- Zalesky A, Fornito A, Bullmore ET (2010): Network-based statistic: Identifying differences in brain networks. *NeuroImage* 53:1197–1207.
- Zhang D, Liu X, Chen J, Liu B, Wang J (2015): Widespread increase of functional connectivity in Parkinson's disease with tremor: A resting-state fMRI study. *Front Aging Neurosci* 7:6.

- Zhang J, Wang J, Wu Q, Kuang W, Huang X, He Y, Gong Q (2011): Disrupted brain connectivity networks in drug-naive, first-episode major depressive disorder. *Biol Psychiatry* 70: 334–342.
- Zhu Y, Bai L, Liang P, Kang S, Gao H, Yang H (2016): Disrupted brain connectivity networks in acute ischemic stroke patients. *Brain Imag Behav.*
- Zhu Z, Fan Y, Feng G, Huang R, Wang S (2013): Large scale brain functional networks support sentence comprehension: Evidence from both explicit and implicit language tasks. *Plos One* 8:
- Zhu Z, Zhang JX, Wang S, Xiao Z, Huang J, Chen HC (2009): Involvement of left inferior frontal gyrus in sentence-level semantic integration. *NeuroImage* 47:756–763.